



CHORUS

This is the accepted manuscript made available via CHORUS. The article has been published as:

Fermions and bosons in nonsymmorphic PdSb₂ with sixfold degeneracy

Ramakanta Chapai, Yating Jia, W. A. Shelton, Roshan Nepal, Mohammad Saghayezhian, J. F. DiTusa, E. W. Plummer, Changqing Jin, and Rongying Jin

Phys. Rev. B **99**, 161110 — Published 16 April 2019

DOI: [10.1103/PhysRevB.99.161110](https://doi.org/10.1103/PhysRevB.99.161110)

Fermions and Bosons in Non-symmorphic PdSb₂ with Six-fold Degeneracy

Ramakanta Chapai^{1#}, Yating Jia^{2#}, W. A. Shelton³, Roshan Nepal¹, Mohammad Saghayezhian¹,

J. F. DiTusa¹, E. W. Plummer¹, Changqing Jin^{2*}, and Rongying Jin^{1*}

¹*Department of Physics and Astronomy, Louisiana State University, Baton Rouge, LA 70803, USA*

²*Institute of Physics, Chinese Academy of Science, Beijing, 100190, China.*

³*Cain Department of Chemical Engineering, Louisiana State University, Baton Rouge, LA 70803, USA*

PdSb₂ is a candidate for hosting 6-fold-degenerate exotic fermions (beyond Dirac and Weyl fermions). The nontrivial band crossing protected by the non-symmorphic symmetry plays a crucial role in physical properties. We have for the first time grown high-quality single crystals of PdSb₂ and characterized their physical properties under several stimuli (temperature, magnetic field, and pressure). While it is a diamagnetic Fermi-liquid metal under ambient pressure, PdSb₂ exhibits a large magnetoresistance with continuous increase up to 14 T, which follows the Kohler's scaling law at all temperatures. This implies one-band electrical transport, although multiple bands are predicted by first principles calculations. **By applying magnetic field along the [111] direction, de Haas-van Alphen oscillations are observed with frequency of 102 T. The effective mass is nearly zero ($0.045m_0$) with the Berry phase close to π , confirming that the band close to the R point has a nontrivial character.** Under quasi-hydrostatic pressure (p), evidence for superconductivity is observed in the resistivity below the critical temperature T_c . The dome-shaped T_c versus p is obtained with maximum $T_c^{max} \sim 2.9$ K. We argue that the formation of Cooper pairs (bosons) is the consequence of the redistribution of the 6-fold-degenerate fermions under pressure.

[#]*These authors contributed equally*

^{*}*Corresponding authors: Jin@iphy.ac.cn; rjin@lsu.edu*

The discovery of topological properties in condensed matter started a new era of physics. Many fermionic particles and phenomena predicted in high energy physics are now experimentally observed in topological materials such as Dirac, Weyl, and Majorana particles [1-3]. Their nontrivial topology gives rise to exotic physical properties, opening the door to future electronics with low-power consumption. The nontrivial topology results from crossings of conduction and valence bands. Depending on crystal symmetry, such crossings can result in degeneracy (g) with $g=2, 3, 4, 6,$ and 8 . It is known that $g=2$ corresponds to Weyl fermions and $g=4$ corresponds to Dirac fermions. These fermions have been extensively studied both in condensed matter physics and high energy physics [4-9]. The cases of $g=3, 6,$ and 8 are of particularly interesting as they can only be found in condensed matter systems, having no high energy analogues as constrained by Poincare symmetry [10].

Based on the density functional theory (DFT), PdSb₂ is predicted to have $g=6$, where the degeneracy is stabilized by its non-symmorphic symmetry: $Pa\bar{3}$ [10]. In this space group, there arises 3-fold degeneracy, which is doubled by the presence of time-reversal symmetry resulting in *6-fold degeneracy*. For PdSb₂, the 6-fold degeneracy occurs at the time-reversal invariant R point at the corner of the Brillouin Zone. **Unlike Dirac and Weyl bands with linear dependence with energy, the 6-fold degenerate bands at the R point have quadratic energy dependence [10]. However, non-Abelian Berry curvature is expected under special holonomy [10].** Although PdSb₂ has been structurally characterized in early 1960s [11], its physical properties remain unknown [12]. We have grown PdSb₂ single crystals, confirming its non-symmorphic structure. For the first time, we report its electrical and magnetic properties under various stimuli (temperature (T), magnetic field (H), and **quasi**-hydrostatic pressure (p)). Several interesting properties are discovered: (1) PdSb₂ is a diamagnetic metal with Fermi-liquid ground state under ambient pressure, (2) there is large positive magnetoresistance (MR) without sign of saturation up to 14 T, which obeys Kohler's scaling law, **(3) there are de Haas-van Alphen oscillations with frequency of 102 T when field is applied along the [111] direction, revealing nearly zero effective electron mass and a nontrivial Berry phase,** (4) it becomes superconducting under the application of p with the maximum superconducting transition temperature; $T_c^{max} \sim 2.9$ K, and (5) first principles calculations indicate the change of band structure under pressure, leading to the charge redistribution.

PdSb₂ single crystal growth and phase determination are described in Ref. [13]. All X-ray diffraction (XRD) peaks can be indexed under a Pyrite-type cubic structure (space group 205 ($P\bar{a}3$)) with the lattice parameter 6.464 Å (Fig. S1 (a) [13]); consistent with the previously reported value [21]. The magnetization measurements were performed in a MPMS (*Quantum Design*). At ambient pressure, the electrical properties were measured using the standard four-probe technique in a PPMS-14 T (*Quantum Design*). The resistivity under **quasi**-hydrostatic pressure was measured via the four-probe method using a diamond anvil cell as described in Refs. [13,22,23]. DFT calculations were performed using a plane-wave based approach that incorporates the projected-augmented wave method within the Vienna *ab-initio* simulation package [13,24-26].

Figure 1(a) shows the temperature dependence of the electrical resistivity of PdSb₂ along the *bc* plane (ρ_{bc}). Note ρ_{bc} decreases with decreasing temperature between 2-400 K with $\rho_{bc}(300\text{K})\sim 75.9 \mu\Omega \text{ cm}$ and $\rho_{bc}(2\text{K})\sim 6.6 \mu\Omega \text{ cm}$, indication of good metallicity. At low temperatures, the data can be fitted with $\rho_{bc}(T)=\rho_0+AT^2$ below 60 K with $\rho_0=6.4 \mu\Omega \text{ cm}$ and $A=2.8 \text{ n}\Omega \text{ cm K}^{-2}$ [see inset of Fig. 1(a)]. The T^2 dependence of ρ_{bc} in this non-magnetic system indicates the Fermi-liquid ground state with dominant electron-electron scattering at low temperatures.

PdSb₂ is diamagnetic resulting from atom core contributions (Fig. S1(c) [13]). Applying H either parallel or perpendicular to the current I, we find that there is positive MR. Figure 1(b) displays the transverse (H \perp I) MR_{bc} at indicated temperatures. The MR_{bc} increases with decreasing temperature. At a fixed temperature, the MR increases with increasing field without any sign of saturation, reaching 174% at 2 K and 14 T. For H//I, the MR_{bc} is about one order of magnitude smaller (Fig. S2 [13]).

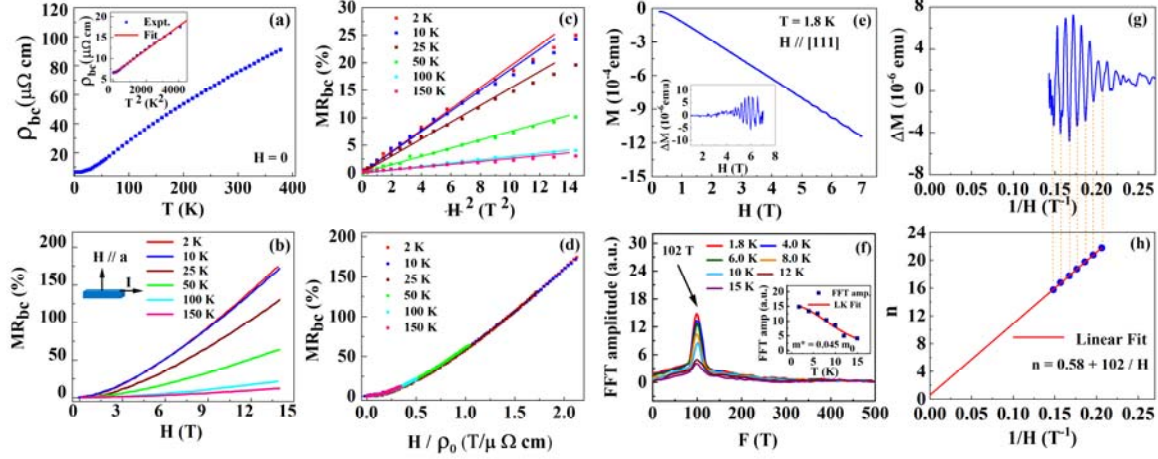


Fig.1. (a) Temperature dependence of the electrical resistivity (ρ_{bc}) of PdSb₂. Inset: ρ_{bc} versus T^2 and fit with $\rho=\rho_0+AT^2$ below 60 K; (b) Transverse MR_{bc} at indicated temperatures; (c) MR_{bc} versus H^2 below 4 T; (d) Kohler plot at indicated temperatures; (e) Magnetization versus field at 1.8 K with $H//[111]$. Inset: ΔM after background subtraction; (f) FFT of oscillatory ΔM at indicated temperatures. Inset: temperature dependence of FFT amplitude and its fit to the Lifshitz-Kosevich formula (see text); (g) ΔM plotted as a function of H^{-1} ; (h) Landau fan diagram constructed from ΔM at 1.8 K. The solid line is the fit of the data using the Onsager Equation.

Since the MR_{bc} for $H//I$ is much smaller than that for $H//I$, there is little contribution from spin scattering. The positive MR in a non-magnetic metallic system is attributed to the modification of electron trajectories due to the application of H . This effect is more significant at low temperatures in pure metallic systems where charge carriers effectively follow the cyclotron motion around the magnetic field [27-30]. By plotting MR_{bc} versus H^2 in Figure 1(c), we find that the MR_{bc} displays quadratic field dependence in the low-field regime (<3 T), as expected for conventional metals with a single band. At higher fields, MR_{bc} gradually deviates from H^2 dependence, while continuously increasing. Such a non-saturating MR has been attributed to exotic mechanisms. For example, MR for the non-symmorphic Dirac semimetal Cd₃As₂ continuously increases up to 65 T, which is attributed to mobility fluctuations [31]. The MR of Cd₃As₂ also scales with H/ρ_0 [31], indicating an effective single-band transport. For PdSb₂, the MR_{bc} data taken at different temperatures collapses into a single curve when plotting MR_{bc} versus H/ρ_0 as shown in Figure 1(d). This implies that Kohler's law is valid for PdSb₂ as well, which is for a single-band transport scenario [30, 31]. Although calculations (Fig. 2 and [10]) indicate the multiband nature of PdSb₂, it appears that only one band plays a dominant role in

electrical transport. In fact, the effective single-band transport in multiband systems is a common feature of topological materials [31].

While there is no sign for quantum oscillations when field is applied along the principle axes of crystals, we have observed such oscillations when the magnetization (M) is measured along the high-symmetry Γ -R direction. Fig. 1(e) shows H dependence of M along the [111] direction at 1.8 K; which exhibits oscillatory behavior with increasing H. The magnetization ΔM after subtracting a smooth background is shown in the inset of Fig. 1(e). The application of a fast Fourier transformation (FFT) to ΔM yields a single frequency $F = 102$ T (Fig. 1(f)) for all temperatures. The FFT amplitude decreases with increasing temperature. The temperature dependence of the FFT amplitude is used to determine the effective mass m^* of electrons

residing in this Fermi surface using the Lifshitz-Kosevich equation [32] $FFT(T) = \frac{A' \left(\frac{m^*}{m_0}\right) T}{\sinh(A' \left(\frac{m^*}{m_0}\right) T)}$

($A' = \frac{2\pi^2 k_B m_0}{e \hbar \bar{H}}$, m_0 is the free electron mass, and \bar{H} is the average magnetic field for our applied field range). The fit of this equation to our data yields $m^* = 0.045 m_0$. This value is close to what is obtained in Cd_3As_2 [31] and Weyl semimetal BaMnSb_2 [7].

The same frequency is obtained if ΔM is plotted as a function of $1/H$ as displayed in Fig. 1(g). Based on the observed oscillations, the Landau fan diagram can be constructed by assigning the minimum ΔM to $n-1/4$ [33], where n is the Landau level index. As shown in Fig. 1(h), $n(H^{-1})$ can be described as $n = 0.58 + 102/H$. This implies that $\Phi_{\text{Berry}} = 0.58 * 2\pi \sim 1.16\pi$ [33], corresponding to a nontrivial Berry phase. The slightly large Φ_{Berry} (compared to π) could be due to errors in determining the minimum ΔM , where there may be another oscillation with smaller amplitude and lower frequency. However, to determine this low-frequency oscillation requires further measurement above 7 T. Additionally, from the Onsager relation $F = (\Phi_0 / 2\pi^2) S_F$ (Φ_0 is the flux quanta), we can estimate the extreme Fermi surface area (S_F) normal to the [111] direction $\sim 0.98 \text{ nm}^{-2}$, corresponds to a small Fermi wave vector $k_F \sim 0.055 \text{ \AA}^{-1}$.

To further understand the observed properties, the electronic structure is calculated using the DFT and shown in Figure 2(a). Consistent with previous results [10], there are 3 bands crossing the Fermi level (E_F) with contributions from both Pd and Sb. At the R point, there is a 6-fold degeneracy, marked by a circle in Figure 2(a). Three bands are congregating at the R point as the non-symmorphic symmetry protects this degeneracy. Since all of them are doubly

degenerate due to the inversion symmetry, *6-fold degeneracy exists at the R point*. In addition, we find that Sb dominates the band structure around E_F (Table S1 [13]).

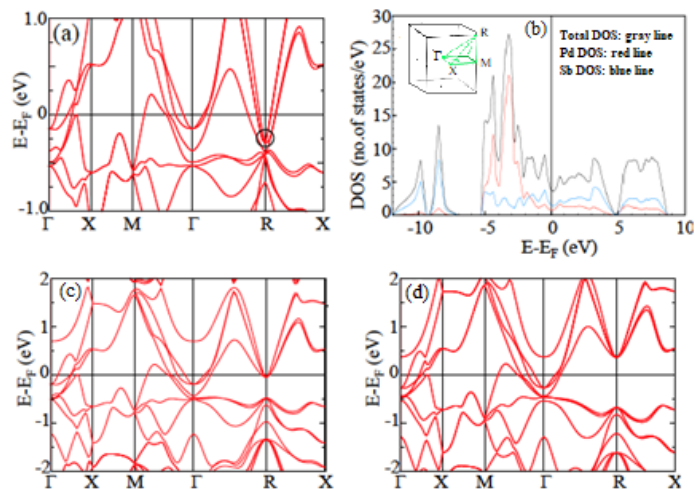


Fig.2. (a) Electronic structure near the Fermi level. (b) Density of states (DOS) from Pd (red), Sb (blue) and the sum. Inset: the first Brillouin zone of PdSb₂; (c-d) Band structure under p=17.66 GPa and 45.60 GPa, respectively.

The above analysis indicates that the topological states near E_F at the Γ and R points are primarily coming from Sb (between -0.37 eV and E_F). The DOS plots shown in Figure 2(b), show that there is a crossover at ~ -1.5 eV where the site-projected Sb DOS overtakes the Pd site-projected DOS, indicating that on the more global scale that there is a larger contribution of Sb states near E_F compared to the Pd states. Furthermore, the effective masses of the three bands at R point are much lighter than bands located at Γ point. This indicates that the latter has higher DOS than that in the R point. Subsequently, the larger contribution of Sb than Pd to the DOS near E_F suggests that the two lightest bands at R point are from Pd.

DFT calculations clearly show that there are both electron and hole bands across E_F . To figure out which band plays a dominant role in electrical transport, we measured the Hall resistivity (ρ_{xy}) at various temperatures. As shown in Figure 3(a), ρ_{xy} exhibits linear field dependence with positive slope $\rho_{xy} = R_H H$ at all temperatures implying hole dominant charge carriers, and behave like single-band situation. The latter is in agreement with the Kohler's scaling behavior. The hole concentration estimated through $\rho_{xy} = R_H H$, as shown in Figure 3(b), decreases with decreasing temperature, reaching $2.5 \times 10^{21}/\text{cm}^3$ at 2 K. The concentration of charge carriers is consistent with the good metallic behavior of PdSb₂ observed. According to

$\mu_H = R_H/\rho$, the Hall mobility μ_H is calculated, which is shown in Figure 3(b). With decreasing temperature, μ_H increases, reaching $380 \text{ cm}^2\text{V}^{-1}\text{s}^{-1}$ at 2 K. This value of mobility is two orders of magnitude lower than that of Cd_3As_2 ($8 \times 10^4 \text{ cm}^2\text{V}^{-1}\text{s}^{-1}$) [8]. Since the resistivity of PdSb_2 is lower than that of Cd_3As_2 , the lower μ_H is due to the higher n in PdSb_2 .

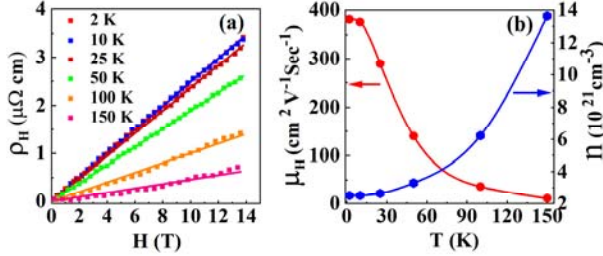


Fig.3. (a) Hall resistivity ρ_H measured at different temperatures and corresponding linear fits (solid lines); (b) Temperature dependence of the Hall mobility μ_H (red) and carrier concentration n (blue).

Since the electrical transport properties of PdSb_2 are governed by carriers residing in one of the hole bands at the ambient pressure, would the electronic structure change under pressure? Figures 2(c-d) show the band structure under 17.66 GPa and 45.60 GPa respectively. While heavy bands (Γ point) remain almost intact, the degenerate light bands (R point) are gradually pushed upward. Above ~ 17.66 GPa, the light bands no longer cross E_F , as shown in Figure 2(d). This indicates that the DOS decreases with increasing pressure (Fig. S4 [13]). Moreover, a Bader charge analysis performed for $p=0$ and 45.60 GPa indicates that, under pressure, Pd gains charge while Sb loses charge, although the Bader volume is larger for Sb (Table S2 [13]).

To probe the effect of the band shift with pressure, we performed the electrical resistivity measurements between 2-300 K under quasi-hydrostatic pressure up to 52 GPa. While the temperature dependence remains similar to that at ambient pressure, the magnitude of ρ tends to decrease with increasing pressure. Upon increasing p , there is little change in ρ in p_1 ($=5$ GPa) $< p < p_2$ ($=35$ GPa), as seen in Figures 4(a-b). Remarkably, above p_2 , two dramatic features are observed: (1) the magnitude of ρ increases with increasing p , and (2) there is sharp resistivity drop with $p \geq 41$ GPa. Below, we quantitatively analyze these two features.

Under pressure, we find that ρ continuously follows T^2 temperature dependence at low temperatures. We thus fit the low-temperature $\rho(T)$ using the same formula as that for the

ambient pressure case. Figure 4(c) displays both residual resistivity ρ_0 and coefficient A under pressure. After initial drop, ρ_0 increases with increasing p when $p \geq 2.6$ GPa, with larger slope when $p > p_2$. The increase of ρ_0 with pressure may be because of the increased scattering with impurities in the squeezed environment. On the other hand, the coefficient A initially decreases then increases after reaching the minimum at p_2 . It further decreases after reaching the maximum at $p_3 \sim 47$ GPa. Within the Fermi-liquid theory, A is proportional to DOS. The non-monotonic pressure dependence of A implies the non-monotonic variation of DOS. This suggests that the shift of 6-fold-degenerate bands to higher energy by pressure (Figures 2(c-d)) involves charge transfer, thus changing the DOS. **It should be pointed out that our XRD measurements under pressure show no evidence of any structural phase transition (Fig. S3 [13]).**

To confirm the change of DOS under pressure, we measured the pressure dependence of ρ_H at 20 K. While the field dependence of ρ_H is linear with positive slope as seen in Figure 3(a), the slope R_H depends on p . Figure 4(d) shows the pressure dependence of n converted from R_H , which varies non-monotonically. There is a kink at p_1 , a local maximum at p_2 , and a minimum at p_3 . The change of n reflects electron redistribution under pressure. **Given the overall similar $\rho(T)$ profile under the wide range of pressure, the dominant hole carriers should be from the doubly degenerate band starting ~ -0.6 eV at the X point that has hole pocket between the M and Γ (Fig.2(a)).**

We now turn to the sharp resistivity drop at low temperatures and high pressure which is shown in Figure 4(e). Note that there is obvious drop at 41 GPa. Although not reaching zero, the resistivity drop becomes sharper under higher pressure. This suggests that the system undergoes a superconducting transition. We determine the critical temperature T_c , at which ρ reduced to 90% of its normal value. As plotted in Figure 4(f), T_c initially increases then decreases after reaching maximum at p_3 . Since $T_c = 1.2$ K is expected at ambient pressure [12], there may be a superconducting dome as shown in Figure 4(f).

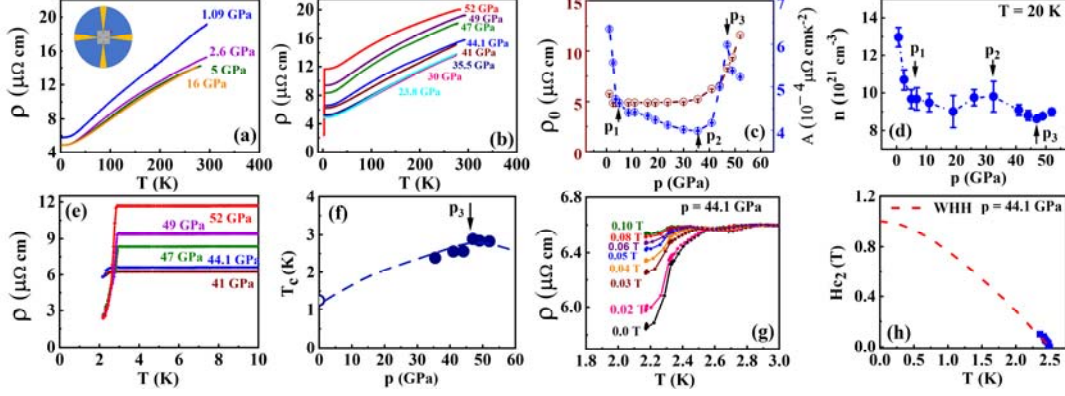


Fig.4. (a-b) Temperature dependence of ρ under pressure. Inset: schematic configuration of electrodes on the sample; (c) Pressure dependence of ρ_0 and A (see text); (d) Pressure dependence of n at $T=20$ K; (e) Temperature dependence of ρ showing superconducting transition; (f) Pressure dependence of T_c , where the dashed line is to guide the eye based on information in Ref. [12]; (g) Temperature dependence of ρ under 44.1 GPa at indicated magnetic fields; (h) Temperature dependence of H_{c2} at 44.1 GPa. The dashed line represents the WHH prediction based on the slope at $T_{c0} \sim 2.5$ K.

To further check the origin of resistivity drop, we apply magnetic field at $p=44.1$ GPa. As shown in Figure 4(g), the resistivity drop is reduced upon the application of field, consistent with the scenario of a superconducting transition. The T_c value at each field is plotted as the upper critical field H_{c2} versus T . Using the initial slope $dH_{c2}/dT|_{T=T_{c0}} \sim -0.58$ T/K, we further estimate the $H_{c2}(T=0$ K) ~ 1 Tesla using the Werthamer-Helfand-Hohenberg (WHH) approximation [34].

In view of pressure dependence of quantities shown in Figure 4, one may note that, at p_3 , T_c and A reach the maximum while n reaches minimum. This implies that strong electron-electron interactions (large A) in the environment of reduced carrier concentration favors superconductivity. Within the BCS theory, T_c is determined by the Debye frequency, DOS, and electron-phonon coupling strength. Since $\rho(T)$ profile is unchanged over a wide temperature range, we may assume that there is no dramatic change in Debye frequency with pressure. This again points to the electronic origin for superconductivity.

In conclusion, we have successfully synthesized high-quality PdSb₂ single crystals with the non-symmorphic symmetry. Our first principles calculations confirm that PdSb₂ hosts 6-fold-degenerate fermions with a degeneracy stabilized by the non-symmorphic symmetry. **By applying field along the high symmetry [111] direction, de Haas-van Alphen oscillations with $F=102$ T are observed, corresponding to a band residing electrons with nearly zero effective mass ($0.045m_0$) and a nontrivial Berry phase (1.16π).** In addition to large and non-saturated

magnetoresistance under magnetic field, the application of **quasi**-hydrostatic pressure modifies the electronic structure and changes superconducting transition temperature with $T_c^{max} \sim 2.9$ K at $p_3 \sim 47$ GPa. Interestingly, the normal-state resistivity under pressure behaves similarly to that at ambient pressure, and follows Fermi-liquid behavior at low temperatures prior to the entrance of superconducting state. At T_c^{max} , the coefficient A shows the maximum as well, while the carrier concentration reaches minimum. This suggests that the formation of Cooper pairs (bosons) is the consequence of strong electron-electron interaction. Our discovery of nearly massless electrons with nontrivial Berry phase and superconductivity in a 6-fold-degenerate material offers a unique system to study the behavior of both fermions and bosons.

References

1. Z. K. Liu, B. Zhou, Y. Zhang, Z. J. Wang, H. M. Weng, D. Prabhakaran, S.-K. Mo, Z. X. Shen, Z. Fang, X. Dai et al., *Science* **343**, 864 (2014).
2. V. Mourik, K. Zuo, S. M. Frolov, S. R. Plissard, E. P. A. M. Bakkers, and L. P. Kouwenhoven, *Science* **336**, 1003 (2012).
3. B. Q. Lv, H. M. Weng, B. B. Fu, X. P. Wang, H. Miao, J. Ma, P. Richard, X. C. Huang, L. X. Zhao, G. F. Chen et al., *Phys. Rev. X* **5**, 031013 (2015).
4. B. Q. Lv, Z. -L. Feng, Q. -N. Xu, X. Gao, J. -Z. Ma, L. -Y. Kong, P. Richard, Y. -B. Huang, V. N. Strocov, C. Fang et al., *Nature* **546**, 627 (2017).
5. P. B. Pal, *Am. J. Phys.* **79**, 485 (2011).
6. D. Singh, N. Mobed, and G. Papini, *Phys. Rev. Lett.* **97**, 041101 (2006).
7. S. Huang, J. Kim, W. A. Shelton, E.W. Plummer, and R. Jin, *Proc. Natl. Acad. Sci. USA* **114**, 6256 (2017).
8. T. Liang, Q. Gibson, M. N. Ali, M. Liu, R. J. Cava, and N. P. Ong, *Nature Mater.* **14**, 280 (2014).
9. M. Yan, H. Huang, K. Zhang, E. Wang, W. Yao, K. Deng, G. Wan, H. Zhang, M. Arita, H. Yang et al., *Nature Commun.* **8**, 257 (2017).
10. B. Bradlyn, J. Cano, Z. Wang, M. G. Vergniory, C. Felser, R. J. Cava, and B. A. Bernevig, *Science* **353**, 5037 (2016).

11. S. Furuseth, K. Selte, and A. Kjekshus, *Acta Chem. Scand.* **19**, 735 (1965).
12. In B. T. Matthias, T. H. Geballe, and V. B. Compton's paper in *Rev. Mod. Phys.* **35**, 1 (1963), PdSb₂ is listed as a superconductor with T_c = 1.2 K. However, there is no data to support such claim.
13. See Supplemental material for the sample growth process, crystal structure and magnetization, comparison of transverse and longitudinal MR, characterization under pressure, band structure calculations and site contribution to the wave function at Γ and R points of the Brillouin zone (which includes Refs. [14-20]).
14. H.K. Mao, J. Xu, and P.M. Bell, *J. Geophys. Res.* **91**, 4673 (1986).
15. A. P. Hammersley, S. O. Svensson, M. Hanfland, A. N. Fitch, D. Hausermann, *High. Pres. Res.* **14**, 235 (1996).
16. J. P. Perdew, K. Burke, and M. Ernzerhof, *Phys. Rev. Lett.* **77**, 3865 (1996).
17. W. Tang, E. Sanville, and G. Henkelman, *J. Phys.: Condens. Matter* **21**, 084204 (2009).
18. E. Sanville, S. D. Kenny, R. Smith, and G. Henkelman, *J. Comp. Chem.* **28**, 899-908 (2007).
19. G. Henkelman, A. Arnaldsson, and H. Jónsson, *Comput. Mater. Sci.* **36**, 354-360 (2006).
20. M. Yu and D. R. Trinkle, *J. Chem. Phys.* **134**, 064111 (2011).
21. N. E. Brese, and H. G. Schnering, *Z. Anorg. Allg. Chem.* **620**, 393 (1994).
22. J. L. Zhang, S. J. Zhang, H. M. Weng, W. Zhang, L. X. Yang et al., *Proc. Natl. Acad. Sci.* **108**, 24 (2011).
23. S.J. Zhang, J. L. Zhang, X. H. Yu, J. Zhu, P.P. Kong et al., *J. Appl. Phys.* **111**, 112630 (2012).
24. G. Kresse, and J. Furthmüller, *Phys. Rev. B* **54**, 11169 (1996).
25. G. Kresse, and D. Joubert, *Phys. Rev. B* **59**, 1758 (1999).
26. P. E. Blöchl, *Phys. Rev. B* **50**, 17953 (1994).
27. F. J. Blatt, *Physics of electronic conduction in solids* (McGraw-Hill, New York, 1968).
28. A. A. Abrikosov, *Fundamentals of the Theory of Metals* (North-Holland, Oxford, 1988).
29. S. W. Van Sciver, *Low Temperature Materials Properties. In: Helium Cryogenics. The international cryogenics monograph series* (Springer, Boston, 1986).
30. A. B. Pippard, *Magnetoresistance in Metals* (Cambridge Univ. Press, Cambridge, 1989).

31. A. Narayanan, M. D. Watson, S.F. Blake, N. Bruyant, L. Drigo, Y. L. Chen, D. Prabhakaran, B. Yan, C. Felser, T. Kong et al., *Phys. Rev. Lett.* **114**, 117201 (2015).
32. I. M. Lifshitz and A. M. Kosevich, *Sov. Phys. JETP* **2**, 636 (1956).
33. D. Shoenberg, *Magnetic Oscillations in Metals* (Cambridge University Press, 2009).
34. N. R. Werthamer, E. Helfand, and P. C. Hohenberg, Temperature and purity dependence of the superconducting critical field, H_{c2} . III. Electron spin and spin-orbit effects. *Phys. Rev.* **147**, 295 (1966).

Acknowledgements

This material is based upon work supported by the US Department of Energy under EPSCoR grant DE-SC0012432 with additional support from the Louisiana Board of Regents. The high-pressure experiment at Institute of Physics, Chinese Academy of Sciences was supported by China NSF and MOST research projects.